Journal of the Ceramic Society of Japan 121 [8] 619-622 2013 Paper

Micro/Crystal structure analysis of CSD derived porous $LaNiO_3$ electrode films

Naonori SAKAMOTO,[*,,†] Kotaro OZAWA,[**] Tomoya OHNO,[***] Takanori KIGUCHI,[****] Takeshi MATSUDA,[***] Toyohiko KONNO,[****] Naoki WAKIYA[*,**] and Hisao SUZUKI[*,**]**

[*]Research Institute of Electronics, Shizuoka University, 3–5–1 Johoku, Naka-ku, Hamamatsu 432–8561, Japan
[**]Department of Materials Science and Chemical Engineering, Shizuoka University, 3–5–1 Johoku, Hamamatsu 432–8561, Japan
[***]Department of Materials Science, Kitami Institute of Technology, 165 Koen-cho, Kitami, Hokkaido 090–8507, Japan
[****]Institute for Materials Research, Tohoku University, 2–1–1 Katahira, Aoba-ku, Sendai 980–8577, Japan

$LaNiO_3$ (LNO) is one of an excellent candidate for oxide electrodes especially for perovskite ferroelectric films since it is perovskite type crystal structure, and therefore it is suitable for lattice matching with conventional perovskite ferroelectrics, $Pb(Zr,Ti)O_3$ (PZT), $BaTiO_3$ (BTO), etc. We have been investigating an effect of thermal expansion of the LNO film as PZT/LNO/Si and BTO/LNO/Si structures, where ferroelectric and piezoelectric properties can be improved by a compressive thermals stress implied from the LNO layer to the ferroelectric films. The ferroelectric films also shows high [001] orientation owing to [100] orientation of the LNO film. In the present study, microstructures and crystal structures of the LNO films fabricated on Si substrates by CSD method is investigated by X-ray Diffraction (XRD), field emission scanning electron microscopy (FE-SEM) and transmission electron microscopy (TEM) in order to understand self-orientation along [100] perpendicular to the film plane. The results obviously indicate that the 1 layer deposited LNO film has almost no orientation, whereas it shows tendency of orientation of [100] perpendicular to the film plane when the layer number increased (upto 4 layers). TEM analysis also shows in-plane tensile stress applied to the LNO film is effectively decreased by porous LNO structure, which leads in-plane compressive stress to the ferroelectric films prepared on the LNO films.

Key-words : Film, Stress, Perovskite, Electrode, Orientation

[Received April 16, 2013; Accepted May 23, 2013]

1. Introduction

Perovskite type ferroelectric oxides such as lead zirconate titanate (PZT), barium titanate (BTO) etc. exhibit excellent dielectric, piezoelectric, and ferroelectric properties. Among these materials, PZT films have wide applicability in many fields, such as nonvolatile memories, piezoelectric sensors, and micro-actuators in micro- electro-mechanical systems (MEMS).[1)–4)] PZT possesses superior ferroelectric and piezoelectric properties arisen near the morphotropic phase boundary (MPB) which lies between tetragonal and rhombohedral phases, $PbZr_{0.53}Ti_{0.47}O_3$.[5)–8)] There are quite a lot of studies for fabricating PZT thin films by various deposition methods such as pulsed laser deposition (PLD),[9),10)] sputtering, chemical vapor deposition (CVD),[11)] and chemical solution deposition (CSD).[12),13)] Among these processes, CSD method utilized in the present study has several advantages over the other methods, such as the good homogeneity, low cost, precise control of the composition, relatively low processing temperature, and easy film deposition on large-scale substrates by spin coating.

As bottom electrodes for the PZT film, platinum is conventionally used because of its high electrical performance. However, from practical view point, the platinum electrode is not the best material as electrodes since it causes fatigue over a region of 10^6 switching cycles because of a diffusion of oxygen and/or lead into the Si substrate through the Pt electrode. In order to overcome this issue, oxide electrodes such as $LaNiO_3$ (LNO) are widely investigated. Crystal structure of LNO can be ascribed to a pseudo cubic perovskite with lattice constant of 0.386 nm, therefore it is known to enhance crystallization of the perovskite type films such as PZT ($Pb_{0.53}Zr_{0.47}TiO_3$: a = 0.4063 nm and b = 0.4146 nm). In addition, a resistivity of LNO showed in the range from 5 to 10×10^{-4} Ωcm.[14)]

Electrical properties of the ferroelectric thin films are generally influenced by many factors such as crystallinity, orientation, morphology, stresses, composition, electrode structures etc. Among these factors, we have been investigating a stress effect impressed to the film from bottom electrodes and substrates caused by different thermal stresses among them. In our previous report, highly a-/c-oriented PZT thin film deposited on a porous $LaNiO_3$ (LNO) thin film electrode was prepared by chemical solution deposition (CSD) method. It should be noted that ferroelectric properties of the PZT film increased with increasing the LNO layer thickness.[15)] The increased LNO film thickness also resulted in an increase of PZT lattice parameters perpendicular to the film plane, which indicated that the LNO film impressed compressive stress in plane caused by a high thermal expansion coefficient of LNO (12.5×10^{-6}/K)[16)] compared to Si. A mechanism of the compressive stress impression can be thought as follows; the compressive stress is impressed to the PZT film by the high thermal expansion coefficient of the LNO film and simultaneously the tensile stress to the PZT film generally impressed from Si due to different thermal expansion coefficient between LNO and Si is effectively eased by the porous structure of the LNO film.[15)] In the present study, precise investigation of

† Corresponding author: N. Sakamoto; E-mail: tnsakam@ipc.shizuoka.ac.jp

DOI http://dx.doi.org/10.2109/jcersj2.121.619

the LNO films prepared on Si substrates by CSD method was made by transmission electron microscopy (TEM) and field emission scanning electron microscopy (FE-SEM).

2. Experimental procedure

$La(NO_3)_3{\cdot}6H_2O$ and $Ni(CH_3COO)_2{\cdot}4H_2O$ were used as starting materials for preparing the LNO precursor, and a solution of 2-methoxyethanol and ethanolamine was used as a solvent. Prior to preparation of precursors, $La(NO_3)_3{\cdot}6H_2O$ was dried at 150°C for 60 min. and $Ni(CH_3COO)_2{\cdot}4H_2O$ was dried at 150°C for 60 min. and subsequently dried at 200°C for 60 min. 0.3 M La precursor solution was prepared by dissolving the dried $La(NO_3)_3$ into 2-methoxyethanol (25 ml) and stirred for 90 min. at room temperature. 0.3 M Ni precursor solution was prepared by dissolving the dried $Ni(CH_3COO)_2$ into mixed solution of 2-methoxyethanol (20 ml) and ethanolamine (5 ml) and refluxed at 105°C for 30 min. Mixing and stirring the two solutions for 120 min. at room temperature yielded LNO precursor solution of 0.3 M (50 ml). The LNO precursor solution was deposited on a Si substrate by spin-coating at 3500 rpm. The as-deposited LNO thin film was dried at 150°C for 10 min and pre-annealed at 350°C for 10 min in order to remove residual organics. The LNO precursor film was then annealed at 700°C for 5 min by rapid thermal annealing in oxygen atmosphere in order to effectively remove the residual organics in the precursor film. The estimated thickness of the LNO film after one cycle of spin coating was 50 nm. Various thicknesses of LNO films, 50, 100, and 200 nm were prepared.

Microstructures of the thin films were investigated using transmission electron microscopy (TEM, 200 kV, JEM-2100F, JEOL) for Bright field (BF) and field emission scanning electron microscopy (FE-SEM, JSM-7001F, JEOL). Crystalline phases of the obtained film were characterized by X-ray diffraction (XRD, D8 ADVANCE, Bruker AXS GmbH) and selected area electron diffraction (SAED). Diffraction data obtained by the SAED patterns were corrected using Au standard sample. Lattice parameters of the LNO crystals at several areas in the film were measured by the diffraction spots of LNO along horizontal/vertical directions of the film plane. Sample preparation for the TEM observation was performed by the ion milling system (Ion slicer, EM-09100IS; JEOL).

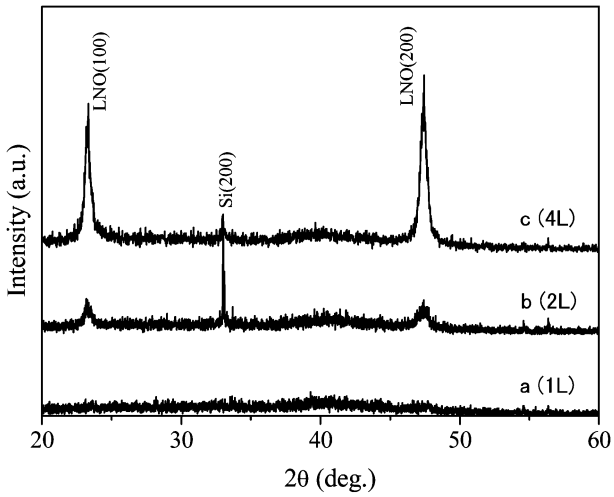

Fig. 1. XRD patterns of the LNO/Si films with various LNO layer thicknesses. (a) 50 nm, (b) 100 nm, and (c) 200 nm.

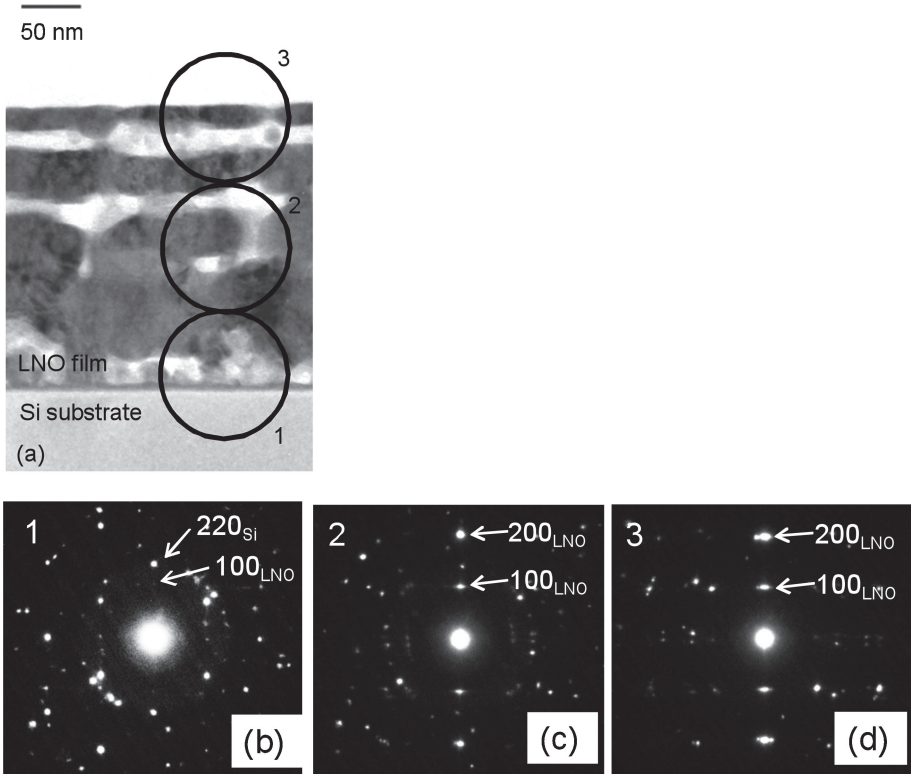

Fig. 2. (a) Cross-Sectional TEM bright field image for LNO/Si thin film with LNO thickness of 200 nm. Porous structures of the LNO layer was observed. (b)–(d) Selected electron diffraction patterns obtained the areas indicated by the circles 1–3 in the TEM image (a). It is obviously understood that intensity of the diffraction spots 100 and 200 of the LNO crystals became strong with increasing the film thickness.

3. Results and discussion

3.1 Crystal orientation

Figure 1 shows XRD patterns for the LNO films prepared on Si substrates. It is obviously understood that the LNO film has [100] orientation perpendicular to the film plane. This orientation is also seen in our previous study, where PZT films were prepared on the LNO film.[15] The peak intensity of the LNO [k00] considerably increased with increasing the film thickness, which implies the [k00] orientation increased with increasing the film thickness as well as merely the film thickness (a mass of the film) increased.

3.2 Cross sectional observation by TEM

Figure 2 shows cross sectional bright field TEM image of the LNO film (4 layers) deposited on Si substrate. It is understood that the LNO film has porous structures composed of 50–100 nm particles. Although the layer structures were not obviously seen, the pores mostly seemed to be connected in-plane and some of the pores (about several tenth nm) penetrated over layers. Electron diffraction patterns taken at the areas indicated by the circles 1 to 3 indicated that the orientation of the LNO [k00] perpendicular to the film plane increased with increasing the film thickness. This result can be confirmed from the results obtained from XRD.

Figure 3 shows lattice parameters of the LNO crystals at each area in the Fig. 2. Although the lattice parameters of the pseudo-cubic LNO crystals should indicates the same values as the bulk one, 0.386 nm, the lattice parameters in the film indicated larger values in-plane, and smaller values out-of plane. One of the most possible reason for the lattice strain is a difference of the thermal expansion coefficient between LNO (12.5×10^{-6}/K) and Si (2.8×10^{-6}/K). Since the LNO film is crystallized at high temperatures, during cooling to the room temperature, the LNO film shrinks more than the Si substrate. Therefore the tensile stress in-plane is applied to the LNO film. The tensile stress, however, was drastically increased with increasing the LNO layers and one can recognize that the LNO films with 200 nm thick was almost stress free. We consider that the reason for such drastic stress buffering is owing to the porous microstructures. As described above, the LNO films were composed of many pores mainly connected along the film plane, therefore the stress was readily buffered within short ranges of 200 nm.

3.3 Surface structures observation by FE-SEM

Figure 4 shows surface images of the LNO films of 1, 2, and 4 layers. One can notice that the LNO films are porous structures in every film. When we precisely observe the surface structures, we also notice that the film has two different shapes of pores, i.e. the large cracks (about 200 nm) with relatively slender shape and small pores (about several tenths to 100 nm) with relatively round shape. It is worth to note that the large cracks decreased and the small pores became clear with increasing the LNO film thickness. With considering the stress state seen in the TEM analysis, it is implied that the large cracks were caused by the cracking due to strong thermal expansion applied to the LNO film, whereas the small pores are the other reasons. The small pores might be resulted from decomposition of the LNO precursor during annealing. As the similar size of small pores were observed in the cross sectional observation, it is also implied that the pores play an important role for buffering the tensile stress applied from the Si substrate.

4. Conclusion

LNO films with different thickness were prepared on the Si substrate by CSD method. The LNO films showed [k00] orientation perpendicular to the film plane. The LNO films showed increasing [k00] orientation with increasing the film thickness. The LNO film was composed of small pores of several tenths to 100 nm in size and the pores effectively buffered the tensile stress in the LNO films applied from Si substrate due to difference of the thermal expansion coefficient between LNO and Si. Surface observation of the LNO film with different thickness indicated

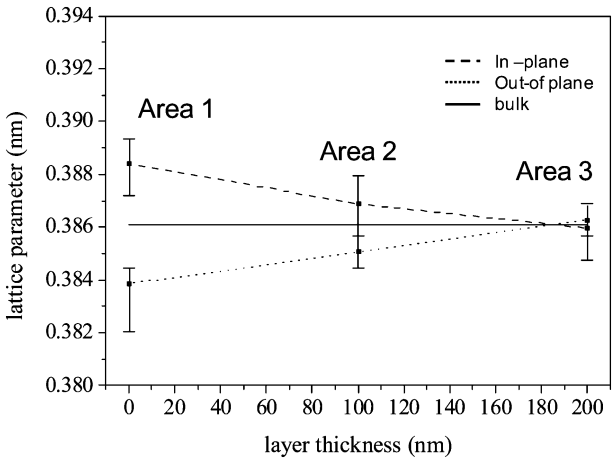

Fig. 3. Lattice parameter changes of the LNO films as a function of the film thickness [area numbers indicates the corresponding areas in the Fig. 2(a)]. The lattice parameters indicated that the tensile stress applied to the LNO films at the interface between the LNO film and the Si substrate decreased with increasing the film thickness and became almost stress free when it reached 200 nm.

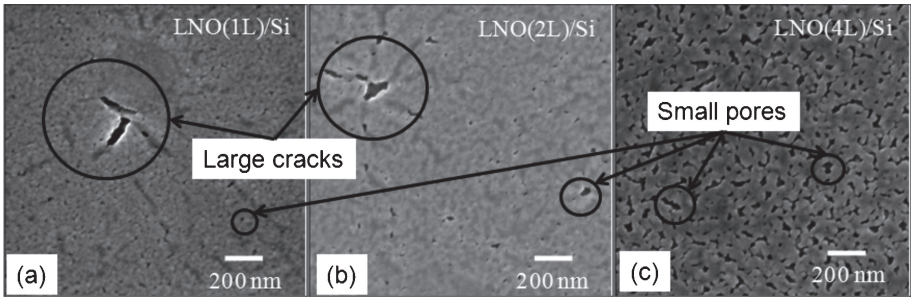

Fig. 4. Surface SEM images of the LNO/Si films with various LNO layer thicknesses. (a) 50 nm, (b) 100 nm, and (c) 200 nm. Thin layer films (50 and 100 nm) showed large cracks of about 200 nm in size, whereas 200 nm thick films showed small pores and no large cracks.

large cracks (about 200 nm) and small pores (about several tenths to 100 nm) were generated on the surface of the LNO films. As the large cracks decrease with increasing the film thickness, the cracks was considered to be formed due to the tensile stress applied to the LNO films. The small pores, on the other hand, seemed to be formed during annealing and played an important role for buffering the tensile stress from the Si substrate.

References

1) P. Muralt, *J. Micromech. Microeng.*, 10, 136–146 (2000).
2) D. V. Taylor and D. Damjanvoic, *Appl. Phys. Lett.*, 76, 1615–1617 (2000).
3) X. Du, J. Zheng, U. Belegundu and K. Uchino, *Appl. Phys. Lett.*, 72, 2421–2423 (1998).
4) S. Li and S. Chen, *Sens. Actuators, A*, 104, 151–161 (2003).
5) S. Serrano, A. Celi and A. Stashans, *Int. J. Nanotechnol.*, 3, 517–526 (2006).
6) X. Sun, Y. Huang and D. E. Nikles, *Int. J. Nanotechnol.*, 1, 328–346 (2004).
7) E. Erdem, M. D. Drahus, R. A. Eichel, H. Kungl, M. J. Hoffmann, A. Ozarowski, J. V. Tol and L. C. Brunel, *Funct. Mater. Lett.*, 1, 7–11 (2008).
8) S. Corkovic, R. Whatmore and Q. Zhang, *Integrated Ferroelectrics*, 88, 93–102 (2007).
9) H. Fujita, S. Goto, M. Sakashita, H. Ikeda, A. Sakai, S. Zaima and Y. Yasuda, *Jpn. J. Appl. Phys.*, 39, 7035–7039 (2000).
10) T. W. Chiu, N. Wakiya, K. Shinozaki and N. Mizutani, *Thin Solid Films*, 426, 62–67 (2003).
11) N. Wakiya, T. Azuma, K. Shinozuka and N. Mizutani, *Thin Solid Films*, 410, 114–120 (2002).
12) H. Miyazaki, Y. Miwa and H. Suzuki, *Mater. Sci. Eng., B*, 136, 203–206 (2007).
13) T. Noda, N. Sakamoto, N. Wakiya, H. Suzuki and K. Komaki, *Mater. Sci. Eng., B*, 173, 25–28 (2010).
14) H. Suzuki, T. Naoe, H. Miyazaki and T. Ota, *J. Eur. Ceram. Soc.*, 27, 3769–3773 (2007).
15) T. Ohno, T. Matsuda, K. Ishikawa and H. Suzuki, *Jpn. J. Appl. Phys.*, 45, 7265–7269 (2006).
16) T. Ohno, B. Malic, H. Fukazawa, N. Wakiya, H. Suzuki, T. Matsuda and M. Kosec, *J. Ceram. Soc. Japan*, 117, 1089–1094 (2009).